

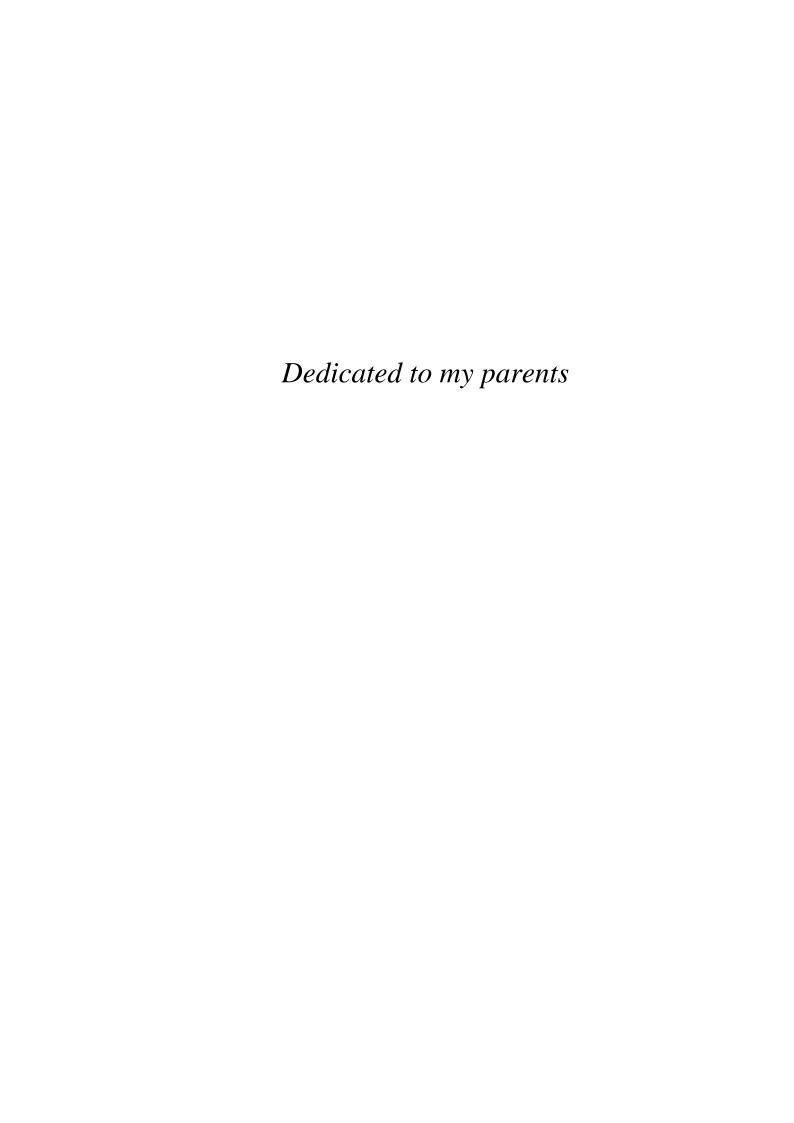
#### THE UNIVERSITY OF ADELAIDE

School of Electrical and Electronic Engineering

# Design of Permanent Magnet Machines for Field-Weakening Operation

**Chun Tang** 

A thesis presented for the degree of Doctor of Philosophy 2015



© 2015 Chun Tang All Rights Reserved



# Design of Permanent Magnet Machines for Field-Weakening Operation

#### **Chun Tang**

Submitted for the degree of Doctor of Philosophy 2015

#### **Abstract**

This research focuses on the electromagnetic design of permanent magnet (PM) machines in terms of the iron loss, torque pulsations and field-weakening performance. It covers the investigation of the effect of stator-slot and rotor-pole number combinations for surface-mounted PM (SPM) machines, and the stator-slot and rotor-effective-slot number combinations for interior permanent magnet (IPM) machines.

The effect of changing the number of slots and poles on the performance of a particular SPM machine design is studied in detail using finite element analysis. This includes examining the back-EMF, the open-circuit/full-load power losses, the cogging/ripple torque, and the field-weakening performance. The simulation results are compared with the expected relationships to provide electric machine designers useful insights on the effect of the number of slots and poles on the performance of SPM machines.

Operation at high speed in traction drives corresponds to deep field-weakening conditions. Due to the high electrical frequencies, the iron loss of IPM machines at high speeds can significantly affect the overall efficiency. This thesis investigates the rotor-

cavity positioning and the combination of stator-slot and rotor-effective-slot number on the eddy-current loss for IPM/reluctance machines operating under deep field-weakening conditions. A new closed-form expression for the stator and rotor eddy-current loss is developed. The optimal barrier-positioning for the minimum total loss and the effect on the eddy-current loss of varying the stator-slot and rotor-effective-slot number are investigated for 1-, 2-, 3- and full-layered rotors.

FEM optimisation and experimental verification of an example IPM machine design are presented. An optimized 30 slot, 4 pole (slot/pole/phase = 2.5) three-layered IPM machine with a significantly reduced iron loss under field-weakening operation is proposed and compared to the baseline 36-slot 4-pole (slot/pole/phase = 3) three-layered IPM machine. The detailed comparison of the optimized and baseline designs using a combination of the analytical, FEM and experimental tests are presented.

.

#### **Statement of Originality**

This work contains no material which has been accepted for any other degree or diploma in any university or tertiary institution, and to the best of my knowledge and belief, contains no material previously published or written by another person, except where due reference has been made.

I give consent to this copy of the thesis, when deposited in the University Library, being made available for loan and photocopying, subject to the provisions of the copyright act 1968.

I also give permission for the digital version of my thesis to be made available on the web, via the University's digital research repository, the Library catalogue, the Australian Digital Thesis Program (ADTP) and also through web search engines, unless permission has been given by the University to restrict access for a period of time.

Signe	l:
Date:	June-29-2015

#### **List of Publications**

- [P1] **C. Tang**, W.L. Soong, T. M. Jahns and N. Ertugrul, "Analysis of Iron Loss in Interior PM Machines with Distributed Windings under Deep Field-Weakening", *IEEE Trans. Ind. Appl.*, 2015 (accepted).
- [P2] C. Tang, W.L. Soong, T. M. Jahns, G.S. Liew and N. Ertugrul, "Analysis of Stator Iron Loss in Interior PM Machines under Open and Short-Circuit Conditions", *IEEE Energy Conversion Congress and Exposition (ECCE)*, 2013, Denver.
- [P3] **C. Tang**, W.L. Soong, G.S. Liew and N. Ertugrul, "Modelling of a Bonded Magnet Ring Surface PM Machine using Soft Magnetic Composites", *Int. Conf. on Elect. Machines (ICEM)*, 2012, France.
- [P4] **C. Tang**, W.L. Soong, G.S. Liew and N. Ertugrul, "Effect of Pole and Slot Number Changes on the Performance of a Surface PM Machine", *Int. Conf. on Elect. Machines (ICEM)*, 2012, France.
- [P5] **C. Tang**, W.L. Soong, P. Freere, M. Pathmanathan and N. Ertugrul, "Dynamic Wind Turbine Output Power Reduction under Varying Wind Speed Conditions Due to Inertia", *Wind Energy* 2012; DOI: 10.1002/we.1507.
- [P6] G.S. Liew, **C. Tang**, W.L. Soong, N. Ertugrul and D.B. Gehlert, "Finite-Element Analysis and Design of a Radial-Field Brushless PM Machine Utilizing Soft Magnetic Composites", *IEEE Int. Electric Machines and Drives Conf. (IEMDC)*, 2011, Canada, pp. 930-935.

- [P7] M. Pathmanathan, **C. Tang**, W.L. Soong and N. Ertugrul, "Detailed Investigation of Semi-Bridge Switched-Mode Rectifier for Small-Scale Wind Turbine Applications", *IEEE Int. Conf. on Sustainable Energy Technologies (ICSET)*, 2008, Singapore, pp. 950-955.
- [P8] **C. Tang**, M. Pathmanathan, W.L. Soong and N. Ertugrul, "Effects of Inertia on Dynamic Performance of Wind Turbines", *Australasian Universities Power Engineering Conference* (AUPEC), Dec. 2008, Australia.
- [P9] M. Pathmanathan, C. Tang, W.L. Soong and N. Ertugrul, "Comparison of Power Converters for Small-Scale Wind Turbine Operation", *Australasian Universities Power Engineering Conference* (AUPEC), Dec. 2008, Australia.

#### Acknowledgements

I would like to thank my supervisor, Prof. Wen L. Soong for all his generous support and expert guidance over all these years both at the professional and personal level. I am also grateful for the help and assistance provided by my co-supervisors, Prof. Nesimi Ertugrul, Dr. Gene Liew and Dr. Peter Freere. I express gratitude towards the University of Adelaide and the Australian Research Council for supporting my studies through the Australian Research Council Discovery grant, DP0988255. I would sincerely like to thank the staff of the Electrical Engineering Workshop for all the time they invested in aiding my projects.

I would also like to thank Prof. Thomas M. Jahns from University of Wisconsin-Madison, for his insightful technical discussions and generous help during the period of my stay in Madison.

Finally, I would like to thank my family for the invaluable support and patience during this journey.

## **Table of Contents**

Abstract	i
Statement of Originality	
List of Publications	
Acknowledgements	vii
Table of Contents	ix
List of Figures	xiii
List of Tables	xvii
Nomenclature	
Acronyms	xxiii
Chapter 1. Introduction	
1.1. Background and Motivation	
1.2. Typical Structures of PM Synchronous Machines	2
1.3. General Electromagnetic Performance Evaluations	2
1.3.1. Power Loss and Efficiency	2
1.3.2. Electromagnetic Torque	
1.3.3. Field-Weakening Performance	
1.3.4. Power-Factor	
1.4. Thesis Overview	4
1.4.1. Research Gap	
1.4.2. Original Contributions	
1.4.3. Thesis Outline	
Chapter 2 Effect of Pole and Slot Number on Performance of SPM Machines	7

2.1. Baseline Design and Analysis Approach	8
2.1.1. 2-D Finite-Element Method to Solve Magnetic Problems	8
2.1.2. Base-Line Machine and Analysis Methodology	9
2.2. Open-Circuit Parameters	12
2.2.1. Back-EMF	13
2.2.2. Open-Circuit Losses	15
2.2.3. Cogging Torque	17
2.3. Full-Load Performance	19
2.3.1. Rotor Iron and Magnet Losses at Rated Current	19
2.3.2. Full-Load Losses	22
2.3.3. Torque Ripple	24
2.4. Field-Weakening Performance	25
2.4.1. Inductance and Characteristic Current	25
2.4.2. Field-Weakening Performance	27
2.5. Conclusion	29
Chapter 3. Analysis of Iron Loss in IPM Machines under Deep Field-Weakening	
3.1. Introduction	
3.1.1. Related Works	
3.1.2. Objectives and Contributions	
3.2. Analytical Eddy-Current Loss Modelling	
3.2.1. Stator and Rotor Magneto-Motive Force	
3.2.1.1. Stator Magneto-Motive Force	
3.2.1.2. Rotor Magneto-Motive Force	
3.2.2. Stator Flux and Eddy-Current Loss Density	
3.2.2.1. Airgap, Stator Yoke and Teeth Flux Density	
3.2.2.2. Stator Yoke and Teeth Eddy-Current Loss Densities	
3.2.3. Rotor Flux and Eddy-Current Loss Densities	
3.2.4. Volumes of Stator and Rotor Iron	
3.3. Optimisation of Rotor-Cavity Positioning	
3.3.1. Analytical Predicted Eddy-Current Loss	
3.3.2. FEM Eddy-Current Loss with Reluctance Rotors	
3.3.3. FEM Eddy-Current Loss with IPM Rotors	
3.4. Optimisation of Stator-Slot and Rotor-Effective-Slot Number Combinations	
3.4.1. Effect of Changing Rotor-Effective-Slot Number	
3.4.2. Effect of Changing Stator-Slot Number	
3.4.3. Effect of Changing Both Stator-Slot and Rotor-Effective-Slot Number	
3.4.4. Selection of Stator to Rotor Slot Number Ratio	
3.5. Conclusion	61
Chapter 4. FEM Optimization and Experimental Verification	63
4.1. FEM Design and Optimisation	

4.1.1. FEM Design of D-Axis Flux Linkage and Torque	66
4.1.2. FEM Design for Iron Loss Reduction	68
4.1.3. FEM Design for Torque Ripple Reduction	71
4.2. Experimental Verification	71
4.2.1. Experimental Verification of FEM Calculated Parameters	
4.2.1.1. Rotor Magnet Remanent Flux Density $B_r$	74
4.2.1.2. Stator End-Winding Inductance <i>L</i> <sub>end</sub>	79
4.2.1.3. Field-Weakening and Short-Circuit Performance	84
4.2.2. Iron Loss Segregation for Open- and Short-Circuit Tests	
4.2.3. Experimental Verification of Stator-Teeth Flux Density and Iron Loss	89
4.3. Conclusion	93
Chapter 5. Conclusion	95
5.1. Summary of Key Results	
5.2. Suggestions for Further Research	99
A.1. "Filter Function" Analysis for Flux and Eddy-Current Loss Density Spectra10	01
A.2. Spectral Analysis of Stator Eddy-Current Loss under Open Circuit Conditions10	04
A.3. Spectral Analysis of Stator Eddy-Current Loss under Deep Field-Weakening 10	06
A.4. Summary for Filtering Effect	08
References	11

# **List of Figures**

Figure 1-1: Example surface-mounted PM and interior PM rotor	2
Figure 2-1: Sketch and mesh of cross-section for an example PM machine	9
Figure 2-2: Cross-sections for the 36- and 12-slot stators	10
Figure 2-3: FE open-circuit flux line plot, spatial airgap flux distribution, stator	
tooth/yoke flux density waveform and back-EMF at 6,000rpm, the airgap	
flux distribution due to stator current and its spatial harmonic spectrum and	
the cogging torque and torque ripple waveforms	11
Figure 2-4: Calculated peak fundamental airgap flux density, analytical winding	
factor, calculated phase fundamental back-EMF at 6,000rpm and rated	
current for the 36- and 12-slot SPM machines	14
Figure 2-5: Calculated stator-slot and end-winding copper loss at rated torque	15
Figure 2-6: Calculated open-circuit loss for the machine designs at 6,000 rpm	16
Figure 2-7: Two cogging torque indices based to the least common multiple of the	
number of slots and poles, and the calculated peak cogging torque for the	
36- and 12-slot machines	18
Figure 2-8: Two proposed rotor loss indices and the calculated solid rotor and un-	
segmented magnet power losses for 36- and 12-slot machines	20
Figure 2-9: Calculated rotor iron and magnet losses showing the effect of	
lamination and magnet segmentation for 12-slot machines at 6,000rpm	21
Figure 2-10: Diagram showing the schemes of segmenting the rotor magnets	22
Figure 2-11: Calculated stator iron and rotor losses for the open-circuit and full-	
load conditions for 36- and 12-slot machines at 6,000 rpm	23

•	total full-load loss for the 36- and 12-slot machines and lculated efficiency at 35 Nm and 6,000 rpm.	24
1 0	peak torque ripple at full-load in comparison to the peak	2 .
<b>U</b>	or the 36- and 12-slot machines	25
	phase back-EMF, reactance and characteristic current of	
•	PM machines at 6000rpm	26
	field-weakening output power versus speed for the 36- and	20
	operating with the same voltage and current limit	28
	owing the deep field-weakening with the optimal operating	20
•	wing the deep field weakening with the optimal operating	32
	ns of rotors with $n_{\rm r} = 18$ , showing examples of 1-, 2- and 3-	34
•		22
=	d the full-layered rotor.	33
= =	showing: the major quantities and reference axes, the	
	le magnetic circuit used for calulating the rotor mmf	
•	soidal stator MMF, the rotor barrier angular locations and	•
	rresponding rotor mmf for a ¼ electric cycle	
· ·	wing the $q$ -axis "tunneling" flux in a rotor channel	
Figure 3-5: Diagram sho	wing the parameters used for calculating iron volumes	47
•	f analysis process for the stator eddy-current loss and the	
rotor eddy-curren	it loss	49
Figure 3-7: The eddy-cu	irrent loss for all the possible rotor-cavity positionings of	
the 1-, 2-, 3- an	d full-layered rotor designs for the stator-slot and rotor-	
effective-slot num	mber, $n_s = 15$ and $n_r = 18$	51
Figure 3-8: FEM analys	sis for the 3-layered IPM rotors for $n_s = 15$ and $n_r = 18$	
obtained by a	adding magnets into the reluctance rotors in Figure 3-7	53
Figure 3-9: The eddy-cu	rrent loss by keeping the same ns15 stator and varying the	
rotor-effective s	lot number with the rotor-cavity positioning for the	
minimum total e	eddy-current loss for each stator-rotor slot combination in	
Figure 3-7 for the	e 1-, 2-, 3- and full-layered rotors	54
<del>-</del>	-current loss by keeping the same rotor (nr18) with the	
•	current loss rotor cavity positioning and varying the stator	
•	he 1-, 2-, 3- and full-layered rotors.	56
	ldy-current loss contours in a plane of $n_r$ versus $n_s$ , with the	
· ·	eddy-current loss rotor-cavity positioning for each stator-	
	ation	57
	urrent loss map in $n_s$ versus $n_r$ for the 1pu loss contours for	
_	-layered rotors; the 1pu loss contours for the full-layered	
	$/n_s$ ratio contours	50
	ddy-current loss versus $n_r/n_s$ ratio for each design with the	30
	eddy-current-loss rotor cavity positioning for each stator-	<i>(</i> 0
rotor slot combin	ation in Figure 3-10.	60

Figure 3-14: The minimum eddy-current loss boundaries in the total eddy-current	
loss versus $n_r/n_s$ ratio highlighted in Figure 3-13	61
Figure 4-1: Cross-section views of stators and rotors showing the four	
combinations: baseline ns18nr12 and optimized ns15nr18, along with	
ns18nr18 and ns15nr12 obtained by interchanging the stators and rotors	64
Figure 4-2: The B-H characteristic from the 35JN250 steel datasheet	66
Figure 4-3: FE <i>d</i> -axis flux-linkage versus <i>d</i> -axis current plot with the initial values	
of magnet remanence $B_r$	67
Figure 4-4: FE average torque versus current angle plot with the initial values of	
magnet remanence $B_r$ ; current amplitude was kept constant at 8.6Arms	67
Figure 4-5: FEM iron loss density contours with $I_d = -8.6$ Arms, $I_q = 0$ Arms	69
Figure 4-6: FEM eddy-current and hysteresis loss of the IPM machines under the	
open and short-circuit conditions at a speed of 3,000rpm	69
Figure 4-7: FEM iron loss breakdowns for the IPM machines under the open and	
short-circuit conditions at a speed of 3,000rpm	69
Figure 4-8: The torque versus rotor angle and the average torque and peak-to-peak	
torque ripple calculated by FEM with $I = 8.6$ Arms, $\gamma = 45^{\circ}$	71
Figure 4-9: The ns18 and ns15 stators, and nr12 and nr18 rotors from left to right	
Figure 4-10: The dynamometer setup showing the test IPM machine, torque	
transducer and induction motor drive	73
Figure 4-11: Line back-emf waveforms and spectra calculated by FEM with the	
inital and corrected magnet $B_r$ in comparison to the experimental result	75
Figure 4-12: Calculated RMS magnet flux linkage versus magnet remanent flux	
density $B_r$ identifying the discrepancy in given $B_r$ value	76
Figure 4-13: The spatial distribution of radial airgap flux density and its	
synchronous component for IPM machines under open circuit	77
Figure 4-14: FE <i>d</i> -axis flux-linkage versus <i>d</i> -axis current plot for the IPM machines	, ,
with the tuned magnet $B_r$	79
Figure 4-15: FE average torque versus current angle with tuned magnet $B_r$ ; current	1 )
amplitude was kept constant 8.6Arms for all machines	79
Figure 4-16: FE total iron loss for IPM machines under open circuit comparing	1 )
results with the initial and tuned magnet $B_r$	70
Figure 4-17: FE total iron loss for IPM machines with $I_d = -8.6$ Arms and $I_q = 0$ Arms	1 9
comparing results with the initial and tuned magnet $B_r$	70
	19
Figure 4-18: Flux linkage versus current for $d$ - and $q$ -axis showing the comparison	01
of corrected FEM and experimental measurements	01
Figure 4-19: The calculated maximum torque as a function of current, average	
torque versus current angle with an operating current equal to characteristic	
current and constant 8.6Arms, with the tuned values of magnet remanence	0.0
$B_r$ and including the end-winding inductance.	
Figure 4-20: dq-axis equivalent circuit for an IPM machine	84

Figure	4-21: Predicted performance of IPM machines operating under short-circuit	
	$(V_{ph} = 0V)$ and field-weakening $(V_{ph} = 240V)$ conditions showing the dq-axis	
	current, torque versus speed and power and losses versus speed	85
Figure	4-22: The windage and friction losses measured by using an induction rotor	
	of similar weight to the IPM rotors	86
Figure	4-23: Procedure of segregating the iron loss under open- and short-circuit	
	conditions using the example ns18nr12 IPM machine	87
Figure	4-24: Measured iron loss versus speed for the open circuit condition	88
Figure	4-25: Measured iron loss versus speed for the short-circuit condition	88
Figure	4-26: The flux density contour plots, experimental and FEM stator tooth	
	flux, spectra and eddy-current loss under open-circuit operation	90
Figure	4-27: The flux density contour plots, experimental and FEM stator tooth	
	flux, spectra and eddy-current loss under short-circuit operation	92
Figure	4-28: Comparison of analytical, FEM and experimental iron loss for open	
	circuit and short circuit for four IPM machines at 3,000rpm	93
Figure	A-1: Spectral analysis procedure to predict the tooth and yoke flux densities	
	and their eddy-current losses from the airgap flux density, using the	
	example ns15nr18 IPM under short-circuit conditions	103
Figure	A-2: Airgap radial flux density, tooth flux density and yoke flux density for	
	the ns18nr12 and ns15nr18 IPM machines.	104
Figure	A-3: Open-circuit flux density spectra for the airgap, stator tooth and yoke	
	for the IPM machines showing the analytical prediction and FEM	105
Figure	A-4: Open-circuit eddy-current loss spectra for the airgap, stator tooth and	
	yoke for the IPM machines	105
Figure	A-5: Short-circuit flux density spectra for the airgap, stator tooth and yoke	107
Figure	A-6: Short-circuit eddy-current loss spectra for airgap, stator tooth and yoke	107

### **List of Tables**

Table 2-1: Key Parameters and Dimensions of the SPM Machines	10
Table 2-2: Fundamental Winding Factor $k_{w1}$	13
Table 4-1: General Dimensions for All Test IPM Machines	64
Table 4-2: Parameters for Stators	65
Table 4-3: Parameters for IPM Rotors	65
Table 4-4: The Correction of Magnet Remanent Flux Density $B_r$	76
Table 4-5: Estimation of Stator End-Winding Inductance	80
Table 4-6: Measured magnet flux linkage and characteristic current for IPM Machines	81

## Nomenclature

$\theta$	Stator circumferential coordinates	elec. deg
$\omega_e$	Synchronous angular frequency	rad/s
$\mu_o$	Magnetic permeability of vacuum	H/m
$a_{j}$	rotor cavity angular position	elec. deg
$\Delta_{s}$	Stator tooth pitch angle	elec. deg
$\Delta_r$	Rotor channel pitch angle	elec. deg
$\xi_j$	Rotor channel circumferential position	elec. deg
δ	Angle between the cavity and <i>d</i> -axis	mech. deg
$\Psi_m$	Magnet flux linkage	Wb
$\Psi_d$	Stator d-axis flux linkage	Wb
$arPsi_q$	Stator q-axis flux linkage	Wb
$\Phi_{ m rem}$	Magnet remanent flux	Wb
$\Phi_{\mathrm{lk}}$	Rotor-rib leakage flux	Wb
$B_g$	Radial airgap flux density	T
$B_{gm}$	Magnet created airgap flux density	T
$B_{gr}$	Rotor-MMF contributed airgap flux density	T
$B_r$	Magnet remanent flux density	T

$B_t$	Stator-teeth flux density	T
$B_y$	Stator-yoke flux density	T
$B_{chl}$	Rotor-channel tunnelling flux density	T
$E_{ph}$	Phase back-EMF voltage	$V_{rms}$
$f_{I}$	Synchronous frequency	Hz
$f_s$	Stator MMF	At
$f_{sh}$	Stator MMF spatial harmonics	At
$f_r$	Rotor MMF	At
$f_{rn}$	Rotor MMF spatial harmonics	At
$g_e$	Effective airgap length	m
h	Stator MMF spatial harmonic order	
$I_m$	Stator peak phase current	$A_{pk}$
$I_d$	Stator d-axis current	$A_{rms}$
$I_q$	Stator q-axis current	$A_{rms}$
$I_{ch}$	Characteristic current	$A_{rms}$
$I_{sc}$	Stator short-circuit current	$A_{rms}$
$k_{sh}$	Stator winding factors	
$k_{w1}$	Synchronous winding factor	
$k_{d1}$	Synchronous winding distribution factor	
$k_{p1}$	Synchronous winding pitch factor	
$k_t$	Stator tooth-pitch-at-airgap to body-width ratio	
$k_y$	Pole-pitch-at-airgap to stator-yoke-thickness ratio	
$k_{chl}$	Rotor channel pitch-at-airgap to width ratio	
$k_e$	Eddy-current loss coefficient	$W/m^3$
$l_{stk}$	Lamination stack length	m
$l_{teeth}$	Stator-teeth radial length	m
$l_{chl}$	Rotor-channel mean length	m
$L_d$	d-axis inductance	Н
$L_q$	q-axis inductance	Н
$L_{end}$	Stator end-winding inductance	Н
n	Rotor MMF spatial harmonic order	
$n_s$	Number of stator slot per pole-pair	

$n_r$	Number of rotor slot per pole-pair	
$N_t$	Number of series turns per phase	
p	Number of pole-pairs	
P	Number of poles	
$p_{eddy}$	Eddy-current loss density	$W/m^3$
$p_{\it teeth}$	Stator-teeth eddy-current loss density	$W/m^3$
$p_{yoke}$	Stator-yoke eddy-current loss density	$W/m^3$
$p_{chl}$	Rotor channel eddy-current loss density	$W/m^3$
$r_g$	Average airgap radius	m
$r_j$	Rotor channel magnetic potential	At
$R_s$	Stator phase resistance	ohms
$R_b$	Rotor barrier magnetic reluctance	$H^{-1}$
$R_g$	Sectional airgap magnetic reluctance	$H^{-1}$
$R_{yoke}$	Stator-yoke average radius	m
$R_{teeth}$	Stator-teeth average radius	m
$R_{rot}$	Rotor outer radius	m
S	Stator slot number	
$T_{ave}$	Total average torque	Nm
$T_{mag}$	Magnet torque	Nm
$T_{rel}$	Reluctance torque	Nm
$V_{ph}$	Stator phase voltage	$V_{rms}$
$V_{yoke}$	Stator-yoke volume	$m^3$
$V_{teeth}$	Stator-teeth volume	$m^3$
$V_{chl}$	Rotor-channel volume	$m^3$
$w_{chl}$	Rotor-channel mean width	m
$w_c$	Cavity thickness	m
$X_d$	d-axis reactance	ohms
$X_q$	<i>q</i> -axis reactance	ohms

### **Acronyms**

CPSR Constant Power Speed Ratio

EMF Electric-Motive Force

FEM Finite-Element Method

FW Field-Weakening

IPM Interior Permanent Magnet

MMF Magneto-Motive Force

MTPA Maximum Torque per Ampere

PM Permanent Magnet

SPM Surface Permanent Magnet

SPP Slots/Pole/Phase

THD Total Harmonic Distortion